energies

MDPI

Article

Design and Thermodynamic Analysis of an Exhaust Gas-Driven LiCl–H_2O Absorption Refrigeration and Heat Pump System for Marine Gas Turbine-Powered Naval Surface Ships

Cüneyt Ezgi [1] and Haydar Kepekci [2,*]

[1] Department of Marine Engineering, Piri Reis University, Istanbul 34940, Turkey; cezgi@pirireis.edu.tr
[2] Department of Mechatronics Engineering, Istanbul Gelisim University, Istanbul 34310, Turkey
* Correspondence: hikepekci@gelisim.edu.tr; Tel.: +90-5394538347

Abstract

This study evaluates an exhaust gas-driven LiCl–H_2O absorption refrigeration and heat pump system for marine gas turbine-powered corvettes and frigates. Recovered exhaust heat drives the cycle, while seawater serves as a heat sink or source depending on the operating mode. Thermodynamic properties have been calculated using Engineering Equation Solver (EES). Increasing solution heat exchanger effectiveness from 0.60 to 0.80 reduced generator heat requirements by 16.97% for the corvette and 13.90% for the frigate. For the corvette, maximum refrigeration and heat pump COP values reached 0.681 and 0.725, with corresponding exergy efficiencies of 0.288 and 0.307. For the frigate, maximum refrigeration and heat pump COP values reached 0.720 and 0.770, with corresponding exergy efficiencies of 0.231 and 0.233. The corvette achieved equivalent fuel savings of 3.129 kg/h, saved fuel costs of 3.880 USD/h, and CO_2 emission reductions of 9.921 kg/h. The frigate achieved equivalent fuel savings of 4.393 kg/h, saved fuel costs of 5.447 USD/h, and CO_2 emission reductions of 13.926 kg/h. Under the fixed operating conditions examined, increased internal heat recovery reduced the generator heat input required for the specified cooling and heating outputs.

Keywords: marine gas turbine; waste heat recovery; LiCl–H_2O absorption refrigeration; heat pump; naval surface ships

Academic Editors: Lei Xi and Denglong Ma

Received: 15 October 2026
Revised: 24 November 2026
Accepted: 25 November 2026
Published: 27 November 2026

Copyright: © 2026 by the authors. Licensee MDPI, Basel, Switzerland. This article is an open access article distributed under the terms and conditions of the Creative Commons Attribution (CC BY) license.

1. Introduction

As maritime transport is a fundamental component of international trade and global supply chains, reducing ships' energy consumption has significant economic and environmental implications [1]. With the expansion of maritime activities, meeting ships' auxiliary energy needs more efficiently, alongside their propulsion requirements, is becoming increasingly important. Energy-saving technologies are therefore a major research area in sustainable transport [2]. Since fuel prices and operating costs directly influence the economic viability of shipboard energy systems, obtaining more useful output from the fuel consumed and reducing auxiliary energy consumption are key objectives in ship operations [3]. Furthermore, reducing CO_2 emissions from maritime transport has become an international priority, requiring improvements in both energy

generation and onboard energy use [4]. Although alternative fuels can contribute to this goal, the investments required for fuel production, supply chain development, and ship retrofitting also necessitate efficiency improvements to existing energy systems [5].

Since not all fuel energy can be converted into mechanical power in the engines and power generation systems used on ships, a significant amount of energy is rejected to the environment through exhaust gases and cooling systems. These streams represent a potential source for energy recovery [6]. Waste heat recovery aims to increase a ship's useful energy output and reduce the additional fuel required to meet the same energy demand by using thermal energy that would otherwise be discarded [7]. Because heat recovered from ship exhaust can be utilized not only for electricity generation but also for cooling through appropriate cycle configurations, waste heat recovery can meet different onboard energy demands simultaneously [8]. However, the choice of recovery technology depends on the heat source temperature, the required useful output, and the ship's operational characteristics. Systems therefore need to be designed for specific operating conditions [9]. Various absorption cycle configurations are being investigated to expand waste heat utilization, as improving the temperature match between the heat source and the cooling demand enables even low-temperature thermal energy to be converted into useful output [10].

Absorption cooling is a refrigeration technology primarily driven by thermal energy, in which a refrigerant is absorbed by an absorbent and subsequently released through heating [11]. A conventional absorption cycle comprises a generator, an absorber, a condenser, an evaporator, a solution pump, and expansion devices. The solution circuit connecting the generator and the absorber allows the refrigerant to be absorbed and released as the solution circulates between these components [12]. The refrigerant released in the generator condenses in the condenser and then produces a cooling effect by evaporating at low pressure in the evaporator. Different arrangements of the evaporation and absorption processes allow the system to meet cooling demands at various temperature levels [13]. Thus, absorption technology offers an alternative to cooling systems based on direct mechanical compression by utilizing available thermal energy. Advanced or combined-cycle configurations can extend the temperature range over which waste heat can be used [14].

Since the operating characteristics of an absorption system are closely linked to the thermodynamic behavior of the refrigerant–absorbent pair employed, the selection of the working pair is a fundamental design decision that must be evaluated alongside the heat source temperature, target cooling conditions, and cycle configuration [15]. Among common working pairs, NH_3–H_2O is suitable for sub-zero cooling applications, whereas H_2O–LiBr is primarily used for chilled water production above 0 °C and air conditioning. Their applications therefore depend on the required cooling temperature [16]. In addition to conventional pairs, alternative refrigerants and ionic liquid-based absorbents are also being investigated. These studies highlight the importance of considering molecular properties, vapor–liquid equilibrium, and cycle performance together when selecting a working pair [17]. Studies of organic refrigerant–absorbent pairs in different cycle configurations show that absorption technology is not limited to these two conventional working pairs. The working pair and cycle configuration can be selected according to the application [18].

The LiCl–H_2O working pair is one of the alternatives evaluated for thermally driven refrigeration and air-conditioning systems, in which water acts as the refrigerant and an aqueous lithium chloride solution serves as the absorbent. The ability of systems using LiCl solutions to operate with low-temperature heat sources provides a basis for investigating this working pair for waste-heat applications [19]. The cooling capacity of absorption systems depends not only on the working pair but also on heat and mass

transfer processes, which depend on solution temperature, concentration, vapor pressure, and cooling conditions [20]. Since internal heat recovery can preheat the solution entering the generator, reducing the required external heat input and affecting energy and exergy performance, it must be considered alongside working pair selection when evaluating the system [21]. Furthermore, selecting the working pair together with the cycle configuration can expand the range of usable heat sources. The suitability of an absorption system should therefore be assessed based on the capacity and energy consumption achieved under specific application conditions, rather than a general ranking of working pairs [22].

In marine applications, the design of waste-heat-driven absorption systems requires both a suitable heat source and a cooling medium to remove heat from the condenser and absorber. Using seawater can reduce the need for freshwater-based cooling infrastructure [23]. Absorption technology can provide both heating and cooling, allowing recovered thermal energy to meet different demands. The system configuration must therefore match these requirements [24]. In this context, a review of waste-heat-driven absorption systems for ships, focusing on heat sources, working pairs, cycle configurations, and performance evaluation methods, helps to compare existing approaches and identify areas requiring further investigation.

Previous studies have investigated waste heat recovery technologies and their integration into marine energy systems. Fisher et al. examined waste heat recovery technologies applicable to power generation, cooling, and energy storage in marine vessels. They highlighted how developing and integrating these technologies into ship energy systems could improve fuel efficiency and reduce emissions [25]. Barone et al. evaluated advanced waste heat management technologies under various operational and environmental conditions. They calculated primary energy savings of approximately 4.5%, 3.5%, and 3% for the Caribbean Sea, the Mediterranean Sea, and the North Sea, respectively, and demonstrated the relationship between recovery performance and the vessel's cooling demand and operating conditions [26]. Diaz-Secades et al. optimized a recovery system that uses heat from a marine engine's exhaust gas, jacket cooling water, lubricating oil, and engine block through preference learning and Bayesian optimization. They found that using this optimized system resulted in a 21.3% increase in power output and a 15.04% increase in fuel efficiency, with reductions of 6.98% in EEXI and 13.85% in CII [27]. Diaz-Secades et al. compared 80 ORC working fluids for marine engine waste heat recovery in terms of power output, efficiency, safety, and environmental impact. In their assessment using preference learning and Bayesian optimization, they reported that R1233zd(E), Novec 649, and SES36 exhibited the best overall performance [28]. Gubba et al. investigated a Joule-cycle-based approach for recovering engine waste heat in marine vessels and heavy-duty vehicles, evaluating a marine engine application using exhaust data for cruise conditions [29]. These studies evaluated shipboard waste heat sources and recovery technologies in terms of energy efficiency, operating conditions, cost, and emissions.

In this context, integrated power and cooling systems have also been investigated for marine applications. Qin et al. combined a supercritical CO_2 recompression Brayton cycle with a transcritical CO_2 refrigeration cycle to utilize waste heat from marine gas turbines. Using multi-objective optimization that accounted for pressure losses, they calculated the COP and waste heat recovery efficiency to be 3.059 and 0.651, respectively [30]. Alkotami et al. integrated a supercritical CO_2 power cycle with multiple organic Rankine cycles to generate power and cooling from the exhaust of marine engines. Their Aspen HYSYS analysis revealed that the net power output increased from 4.91 MW in the reference system to 10.19 MW [31]. Ouyang et al. developed a system driven by waste heat from a marine natural gas engine, comprising a supercritical CO_2 cycle, a transcritical CO_2 Rankine cycle, and a double-effect absorption refrigeration cycle. In their multi-objective

optimization, they determined that using R32 at a mass fraction of 0.6138 in the transcritical cycle yielded the highest net power output (311.6 kW) and the lowest levelized cost of energy (0.0298 USD/kWh) [32]. Que et al. compared four systems for marine applications, involving solid oxide fuel cell–gas turbine units, supercritical CO_2 cycles, and various cooling cycles. They demonstrated that the configuration incorporating an absorption cycle achieved the highest energy efficiency and cooling capacity among the systems studied, at 77.35% and 86.39 kW, respectively [33]. In these studies, power and cooling cycles were combined to generate electricity and cooling from shipboard waste heat.

More specifically, several studies have examined absorption systems driven by waste heat recovered from engines and flue gases. Chun et al. used the waste heat from a large internal combustion engine to drive an absorption cooling system that cooled and dehumidified the intake air. They constructed a superstructure incorporating various absorption cycles and investigated the optimal system configuration using a genetic algorithm. The optimization identified a single-effect absorption system powered by engine coolant preheated in an exhaust gas heat exchanger as the most suitable option [34]. Mubashir et al. combined a supercritical CO_2 Brayton cycle, an organic Rankine cycle (ORC), and an absorption cooling system to generate power and cooling from the exhaust of an internal combustion engine. They compared three different configurations from thermodynamic and economic perspectives. They identified the configuration in which exhaust heat was used in stages and the absorption system was driven by heat from the ORC turbine outlet as the best-performing option. In two separate optimization problems using a genetic algorithm, they calculated an exergy efficiency of 59.21% and a levelized cost of electricity of 0.063 USD/kWh, respectively [35]. Salilih et al. proposed a membrane condenser system integrated with absorption cooling to recover water and waste heat from flue gas. They utilized the flue gas heat in the absorption-cycle desorber and used the resulting cooling to condense water vapor from the flue gas upstream of the membrane condenser. Thus, they investigated using the same flue gas stream for both cooling production and water recovery [36]. In these studies, absorption systems driven by engine and flue gas waste heat were investigated for intake air cooling, combined power and cooling generation, and water recovery.

Further studies have focused on modeling and optimizing waste heat-driven absorption systems under varying ship operating conditions. Zhang et al. integrated an NH_3–H_2O absorption refrigeration system powered by ship exhaust heat with ice storage and optimized operating strategies for a typical shipping route. They demonstrated that ice storage could reduce the imbalance between cooling production and demand [37]. Radchenko et al. developed a method for cooling engine intake air that distributes waste heat between LiBr absorption chillers and ejector chillers. They found that while chiller dimensions could be reduced by approximately 30%, this reduction resulted in about 10% lower fuel savings over the voyage [38]. Mugabi et al. modeled the integration of a LiBr–H_2O absorption system with scavenge air cooling on an LNG vessel under both steady-state and transient conditions. They calculated fuel savings of approximately 0.1% under transient voyage conditions and found that utilizing excess cooling for air conditioning increased the total equivalent savings to 0.2–0.5%. However, they determined that the payback periods exceeded the vessel's typical service life [39]. Ozturk and Kandemir investigated single- and double-effect LiBr–H_2O absorption refrigeration systems using exhaust waste heat from gas turbines and diesel generators on surface ships. They evaluated the systems under different operating conditions and assessed their potential for fuel savings and economic feasibility [40]. Ezgi designed and thermodynamically analyzed a seawater-cooled H_2O–LiBr absorption heat pump driven by diesel engine exhaust for a naval surface ship. The system provided cooling and heating via secondary

circuits controlled by two four-way, three-position valves, and its performance was compared with that of a vapor-compression heat pump [41].

The effects of working-pair selection and cycle configuration have also been investigated using comparative thermodynamic modeling. Ren et al. developed a MATLAB R2014a-based computational model to compare single-effect absorption refrigeration systems using LiCl–H_2O and LiBr–H_2O. They validated the model against literature data and examined the energy and exergy performance of 50 kW chillers using the two working pairs under off-design conditions. They found that the LiCl–H_2O system performed better, particularly at low generator temperatures or high condenser temperatures, and determined that the optimum hot water inlet temperatures were approximately 83 °C for the LiCl–H_2O system and 98 °C for the LiBr–H_2O system [42]. Lei et al. conducted a thermodynamic analysis of series-parallel and reverse-parallel configurations of compression-assisted double-effect absorption refrigeration systems using LiCl–H_2O and LiBr–H_2O to utilize low-temperature heat sources. By evaluating the effects of the solution distribution ratio and compression ratio, they demonstrated that placing a compressor between the evaporator and the absorber was more effective at expanding the operating range and enhancing performance than positioning it between the generators. With a compression ratio of 2 for both compressors, they obtained COP values exceeding 1.16 for the LiBr–H_2O system and 1.29 for the LiCl–H_2O system at a high-pressure generator temperature of approximately 75 °C [43].

The reviewed literature addresses several aspects of marine waste heat recovery, but the scope of individual studies differs. Ozturk and Kandemir [40] examined exhaust-driven LiBr–H_2O refrigeration systems for surface ships, while Ezgi [41] investigated a seawater-cooled LiBr–H_2O absorption heat pump capable of switching between cooling and heating. Ren et al. [42] and Lei et al. [43] compared LiCl–H_2O and LiBr–H_2O systems under different cycle configurations and operating conditions. However, these studies do not establish how a LiCl–H_2O system configured for marine gas turbine exhaust heat recovery performs in corvette and frigate applications when internal solution heat recovery is varied. This application-specific assessment addresses the research gap.

The proposed system applies the LiCl–H_2O working pair to an exhaust-driven marine refrigeration and heat pump arrangement. Two four-way, three-position valves route the secondary fluids between cooling and heating modes. This switching principle follows an established marine arrangement [41]. The distinction of the present study lies in evaluating its application with LiCl–H_2O, a marine gas turbine exhaust heat source, and the design cooling loads of corvettes and frigates. Seawater removes heat from the absorber in each mode and serves as the condenser heat sink during cooling or the evaporator heat source during heating.

The scientific contribution is the assessment of how solution heat exchanger effectiveness affects generator heat requirements, COP, and exergy efficiency under specified operating conditions. The study also estimates equivalent fuel savings, fuel cost savings, and CO_2 emission reductions for the two vessel applications. Its technological contribution is a thermodynamic assessment of this configuration for shipboard thermal demands. The findings provide design-condition performance estimates rather than experimental evidence or an assessment covering all seawater temperatures and operating profiles.

2. Thermodynamic Analysis

The system description, assumptions, and governing equations are presented to evaluate thermodynamic performance, equivalent fuel savings, fuel cost savings, and CO_2 emission reductions.

2.1. System Description

The design of the proposed exhaust gas-driven LiCl–H_2O absorption refrigeration and heat pump system for a marine gas turbine-powered naval surface ship is shown in Figure 1. The proposed system is designed to provide both cooling and heating on board the ship. The main components of the system are a generator, a condenser, an evaporator, an absorber, a solution heat exchanger, a solution pump, refrigerant and solution expansion valves, an exhaust gas economizer, two four-way, three-position (4/3) valves, fan-coil units, and expansion tanks. Water is used as a refrigerant, while an aqueous LiCl solution serves as the absorbent. The system is driven primarily by waste heat recovered from the marine gas turbine's exhaust gases.

The exhaust gas economizer transfers the recovered thermal energy to a closed water circuit connected to the generator. The heated water enters the generator at state 11, supplies the heat required for refrigerant separation, and returns to the economizer at state 12. In the generator, the dilute LiCl–H_2O solution is heated, causing water to evaporate. Since LiCl is essentially non-volatile, the vapor leaving the generator consists almost entirely of water. The resulting concentrated solution exits the generator at state 4 and passes through the solution heat exchanger. In this component, heat is transferred from the hot concentrated solution to the dilute solution returning from the absorber. This internal heat recovery reduces the generator's heat requirement and improves the system's thermal performance.

The concentrated solution leaving the solution heat exchanger at state 5 is expanded through the solution expansion valve before entering the absorber at state 6. In the absorber, the concentrated LiCl solution absorbs the water vapor arriving from the evaporator at state 10. The absorption process releases heat, which is continuously removed by seawater flowing through the absorber between states 13 and 14. The resulting dilute solution leaves the absorber at state 1. The solution pump then increases its pressure, and the pressurized solution enters the solution heat exchanger at state 2. After being preheated, it returns to the generator at state 3, completing the solution cycle.

The water vapor generated in the generator flows to the condenser at state 7. Heat rejection in the condenser causes the refrigerant vapor to condense. The liquid water leaving the condenser at state 8 passes through the refrigerant expansion valve, where its pressure and temperature decrease. The low-pressure refrigerant enters the evaporator at state 9 and absorbs heat as it evaporates. The resulting water vapor leaves the evaporator at state 10 and enters the absorber, where it is absorbed by the concentrated LiCl solution.

Two 4/3 rotary valves are incorporated into the secondary fluid circuit to switch the system between cooling and heating modes. Each valve has connections to the condenser, evaporator, seawater circuit, and fan-coil circuit. The valves redirect the secondary fluid streams without changing the operating direction of the absorption cycle.

In cooling mode, seawater is directed through the condenser between states 15 and 16 to remove the heat released during refrigerant condensation. At the same time, the fan-coil water is circulated through the evaporator between states 18 and 17. The water is cooled in the evaporator and then supplied to the fan-coil units to meet the vessel's cooling demand. After absorbing heat from the conditioned spaces, the fan-coil water returns to the evaporator to be cooled again.

In heating mode, the positions of the 4/3 valves are changed. Seawater is then directed through the evaporator between states 17 and 18, serving as the low-temperature heat source for the system. The refrigerant extracts heat from the seawater as it evaporates. Simultaneously, the fan-coil water is circulated through the condenser between states 16 and 15. The heat released during refrigerant condensation increases the temperature of the fan-coil water, which is subsequently supplied to the conditioned spaces for heating.

The expansion tanks compensate for changes in the volume of the circulating fluids and help maintain stable pressure within the secondary circuits. The proposed arrangement therefore enables the same absorption system to provide cooling through the evaporator and heating through the condenser. The use of seawater as a heat sink in cooling mode and as a heat source in heating mode eliminates the need for an additional external thermal reservoir. At the same time, recovering waste heat from the gas turbine exhaust reduces the system's external thermal energy requirement.

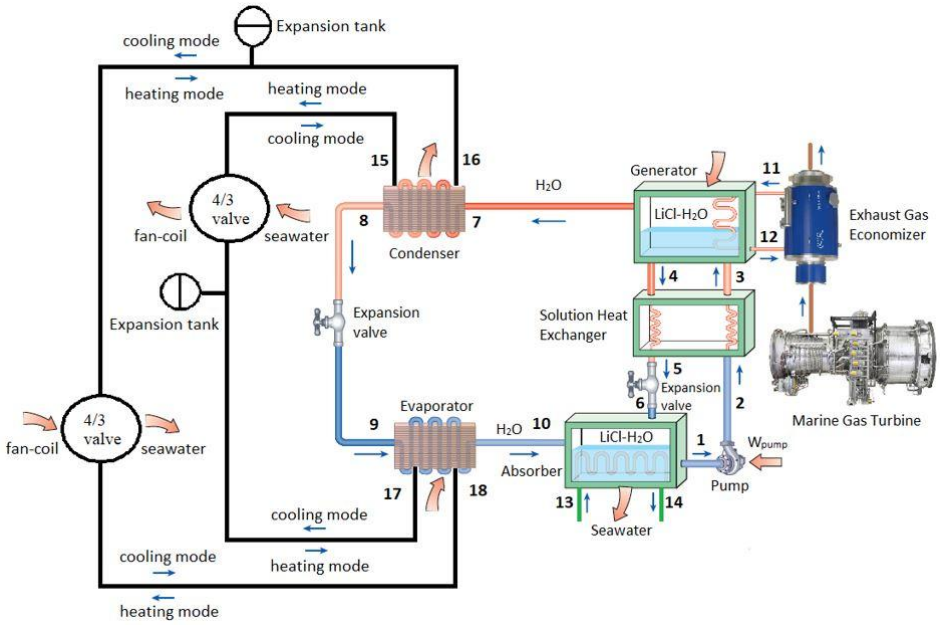


Figure 1. Exhaust gas-driven LiCl–H_2O absorption refrigeration and heat pump system for a marine gas turbine-powered naval surface ship.

The waste-heat sources and design cooling loads considered for the corvette and frigate and the maximum power performance of the LM2500 marine gas turbine (GE Marine, Evendale, OH, USA) are listed in Table 1 and Table 2, respectively.

Table 1. Waste heat sources and design cooling loads for the vessels.

Vessel Type	Waste Heat Source	Design Cooling Load (kW)
Corvette	LM2500 Marine Gas Turbine	540
Frigate	LM2500 Marine Gas Turbine	720

Table 2. Maximum power performance of the LM2500.

Maximum Power Performance	US NSD
Output	22,070 kW
Exhaust gas flow	64.4 kg/s
Exhaust gas temperature	578 °C

2.2. Model Assumptions

The assumptions have been selected to formulate a steady-state thermodynamic model to examine internal heat recovery under specified design conditions. Physical idealizations describe the working pair, component outlet states, and neglected energy transfers. Mathematical simplifications reduce the component models to algebraic mass, species, and energy balances. Prescribed temperatures, cooling loads, and heat exchanger effectiveness values define the cases examined rather than universal operating conditions.

The principal idealizations follow established absorption-cycle modeling approaches [41,42].

a. Steady-state operation.
b. Kinetic and potential energy changes are negligible.
c. Pressure drops and heat losses in piping are negligible.
d. Water is the refrigerant, and the aqueous LiCl solution is the absorbent.
e. LiCl is non-volatile.
f. The generator temperature is fixed at 90 °C.
g. The evaporator temperature is 4 °C.
h. The condenser temperature is 50 °C.
i. The absorber temperature is 35 °C.
j. The generator and condenser operate at 12.35 kPa.
k. The evaporator and absorber operate at 0.8135 kPa.
l. The solutions leaving the absorber and generator are assumed to be in vapor–liquid equilibrium.
m. The refrigerant leaves the condenser as saturated liquid.
n. The refrigerant leaves the evaporator as saturated vapor.
o. The refrigerant and solution expansion processes are isenthalpic.
p. The solution heat exchanger effectiveness varies from 0.60 to 0.80.
q. The analysis is conducted at fixed component temperatures and design cooling loads. Variations in seawater temperature and cooling demand during operation are not included in the model.

The generator, condenser, absorber, and evaporator temperatures of 90, 50, 35, and 4 °C have been selected as reference design conditions consistent with the marine absorption heat pump study of Ezgi [41]. Their adoption does not establish that these temperatures can be maintained under every seawater condition. The pressure levels are determined by the saturation pressures of water at the condenser and evaporator temperatures and are therefore dependent thermodynamic quantities rather than independent assumptions.

Solution heat exchanger effectiveness has been selected as the principal parameter because it determines the extent of internal heat recovery between the concentrated solution leaving the generator and the dilute solution returning from the absorber. Increasing effectiveness raises the temperature of the dilute solution entering the generator and reduces the external heat required for refrigerant separation. This parameter therefore provides a direct basis for examining the influence of internal heat recovery on generator heat input, COP, and exergy efficiency.

Effectiveness values of 0.60, 0.65, 0.70, 0.75, and 0.80 have been examined. The selected interval matches the range discussed for marine absorption heat pumps by Ezgi [41], and the intermediate value of 0.70 has also been used in the LiCl–H_2O analysis by Ren et al. [42]. The increment of 0.05 provides five comparison points within this literature-based interval. Component temperatures and the prescribed cooling load for each vessel are held constant to isolate the effect of effectiveness.

The interval represents a design sensitivity range rather than the measured performance of a particular heat exchanger. Higher effectiveness generally requires greater heat transfer capability, which must be assessed against exchanger size, pressure losses, and cost during detailed design. Cooling of the concentrated solution must also remain compatible with its crystallization limit. These constraints have not been quantified in the present model. Accordingly, 0.80 is the upper value examined, not an established optimum or a verified operating limit.

Thermodynamic properties have been obtained using EES property functions [44].

When modeling a LiCl-water absorption refrigeration and heat pump system, selecting the specific boundary temperatures of 90 °C for the generator, 4 °C for the evaporator, 50 °C for the condenser, and 35 °C for the absorber relies on distinct physical, mathematical, and computational justifications.

From a physical perspective, these values reflect operational realism and environmental constraints. In HVAC applications, chilled water must be delivered at around 7 °C to condition indoor air effectively, which requires the refrigerant water to evaporate at approximately 4 °C to account for heat exchanger temperature differences while remaining safely above water's freezing point at 0 °C. The generator temperature of 90 °C is intentionally chosen to match low-grade waste-heat sources, allowing the cycle to operate without primary fuel consumption. Meanwhile, the absorber temperature of 35 °C, assuming a maximum seawater temperature of 32 °C, and the condenser temperature of 50 °C are dictated by the ultimate heat sink, assuming an incoming heating-water temperature of 40 to 45 °C in heating mode.

From a mathematical perspective, fixing these four temperatures is necessary to achieve thermodynamic closure of the governing equations. Fixing the evaporator and condenser temperatures immediately determines the system's low and high operating pressures using water saturation vapor pressure equations, yielding P_{evap} = 0.8135 kPa and P_{cond} = 12.35 kPa. Furthermore, the generator and absorber temperatures, together with these operating pressures, uniquely determine the concentrations of the strong and weak LiCl solutions via equilibrium relations or Duhring correlations. Once these intensive state properties are known, the model can explicitly solve the coupled mass conservation, species balance, and energy balance equations across each control volume in the cycle.

From a computational perspective, specifying these exact temperatures satisfies the degrees-of-freedom requirements of numerical solvers. A steady-state single-effect absorption model involves a complex system of nonlinear algebraic equations that represent thermodynamic property polynomials and conservation laws. By prescribing these four temperatures alongside standard equilibrium and saturation assumptions, the model's degrees of freedom are reduced to zero, creating a well-posed mathematical problem.

These simplifications reduce the required geometric information and avoid transient, distributed flow, and detailed heat and mass transfer calculations. The results should therefore be interpreted within the stated assumptions and operating conditions.

The present model is a steady-state, component-based thermodynamic model rather than a spatially resolved computational fluid dynamics model. Each component is represented by a control volume, and its inlet and outlet states are related through mass, species, and energy balances. Time-dependent initial conditions, including an initial fluid temperature, are therefore not required. The model does not resolve local velocity fields, wall temperature distributions, or surface heat fluxes. Optical boundary conditions are not applicable because no optical or radiative transport model is included.

The thermal operating conditions are specified by the generator, condenser, absorber, and evaporator temperatures of 90, 50, 35, and 4 °C, respectively. These reference temperatures follow the marine absorption heat pump conditions examined in [41]. The high- and low-pressure levels are determined from the saturation pressures of water at the condenser and evaporator temperatures, giving approximately 12.35 and 0.8135 kPa. Pressure losses are neglected within the absorption cycle. The cooling loads of 540 kW for the corvette and 720 kW for the frigate are prescribed design inputs. Refrigerant mass flow rates are determined from the evaporator energy balance rather than from a specified inlet velocity.

The nominal gas turbine exhaust temperature and mass flow rate are 578 °C and 64.4 kg/s, as listed in Table 2. These values characterize the available heat source and do not

represent the generator solution temperature or an imposed surface heat flux. Heat is transferred to the generator through the economizer water circuit. The required generator heat input is calculated from the cycle energy balance.

The environmental reference temperature used in the exergy calculations is 298 K. This value defines the thermodynamic reference environment.

2.3. Thermodynamic Formulation

The following governing equations are used to perform the thermodynamic analysis of the LiCl–H_2O absorption refrigeration and heat pump system on board ships.

The mass balance equation for a general steady-flow system is expressed as:

$$\sum_{in} \dot{m} = \sum_{out} \dot{m} \tag{1}$$

The energy balance equation for a general steady-flow system is expressed as

$$\dot{Q} - \dot{W} = \sum \dot{m}_{out} h_{out} - \sum \dot{m}_{in} h_{in} \tag{2}$$

$$\sum \dot{m}_{in} x_{in} = \sum \dot{m}_{out} x_{out} \tag{3}$$

The mass balance equation and species balance equation in the generator and absorber can be expressed as Equations (4) and (5), respectively:

$$\dot{m}_{ws} = \dot{m}_{ss} + \dot{m}_r \tag{4}$$

$$\dot{m}_{ws} x_{ws} = \dot{m}_{ss} x_{ss} \tag{5}$$

The circulation ratio CR is an important parameter, which is defined as the ratio of the mass flow rate of the weak solution coming from the absorber to the mass flow rate of the refrigerant:

$$CR = m_{ws}/m_r \tag{6}$$

According to Equations (4) and (5), Equation (6) can be expressed as

$$CR = x_{ss}/(x_{ss} - x_{ws}) \tag{7}$$

The COPs of absorption refrigeration and the heat pump are defined, respectively, as

$$COP_{absorption,REF} = \frac{desired\ output}{required\ input} = \frac{\dot{Q}_L}{\dot{Q}_{in} + \dot{W}_{pump,in}} \tag{8}$$

$$COP_{absorption,HP} = \frac{desired\ output}{required\ input} = \frac{\dot{Q}_H}{\dot{Q}_{in} + \dot{W}_{pump,in}} \tag{9}$$

$$COP_{rev,REF} = (1 - T_0/T_s)(T_L/T_H - T_L) \tag{10}$$

$$COP_{rev,HP} = (1 - T_0/T_s)(T_H/T_H - T_L) \tag{11}$$

where T_L, T_H, T_0, and T_s are the thermodynamic temperatures of the refrigerated space, the heated space, the environment, and the heat source, respectively.

Exergy efficiency for refrigerators and heat pumps is defined as

$$\eta_{ex} = COP/COP_{rev} \tag{12}$$

To give a thorough grasp of the analysis, the calculation approach for fuel savings, expenses, and emissions is described after the governing equations have been established. Specific formulas and assumptions about engine performance and operating conditions form the basis of the calculations for fuel savings, cost savings, and emission reductions.

The saved net power can be calculated as

$$\dot{W}_{net} = \dot{W}_{comp} - \dot{W}_{pump} \quad (13)$$

The saved marine diesel fuel consumption (SFC) can be calculated as

$$SFC = \dot{W}_{net}/(H_u.\eta_{DG}) \quad (14)$$

The cost savings can be calculated as

Cost Savings (USD/h) = Fuel Savings (kg/h) × Fuel Cost (USD/kg)

In this study, the fuel cost for NATO F76 is 4.04 USD/gallon in 2026 [45]. The fuel's lower heating value is 42,718.4 kJ/kg.

The emissions reduction is calculated based on the decrease in fuel consumption and the emission factors for carbon dioxide (CO_2) emissions, which are specific to the type of fuel used (NATO F76). The CO_2 emission factor for NATO F76 is 3.17 kg CO_2/kg fuel [46]. The emissions reduction can be calculated as:

CO_2 Emissions Reduction (kg/h) = Fuel Savings (kg/h) × Emission Factor (CO_2/kg fuel)

3. Results and Discussion

This section examines the effects of solution heat exchanger effectiveness on generator heat input, COP, and exergy efficiency for the corvette and frigate. Equivalent fuel savings, fuel cost savings, and CO_2 emission reductions are also compared. The results were obtained at fixed generator, evaporator, condenser, and absorber temperatures of 90, 4, 50, and 35 °C, respectively, with solution heat exchanger effectiveness varying from 0.60 to 0.80.

Figure 2 illustrates the effect of solution heat exchanger effectiveness on the generator heat input.

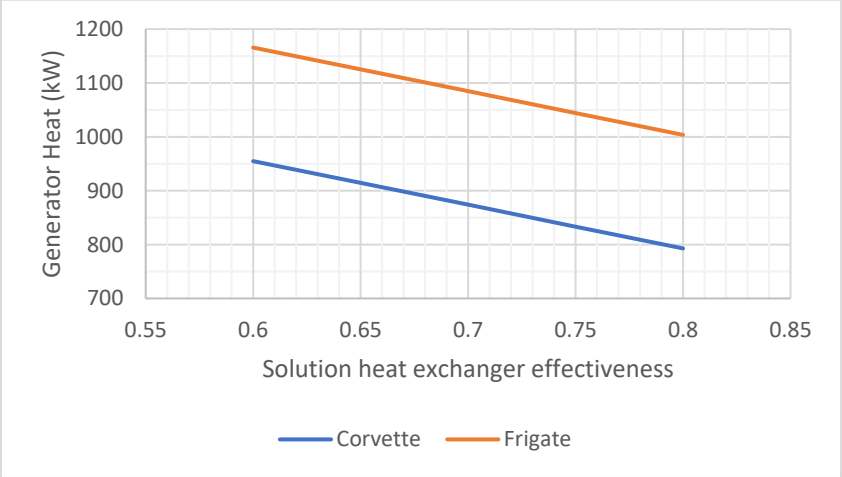


Figure 2. Effect of solution heat exchanger effectiveness on generator heat input for the corvette and frigate.

As the effectiveness increased from 0.60 to 0.80, the generator heat input decreased steadily for both vessels. For the corvette, the generator heat input decreased from 954.91 kW to 792.86 kW, a reduction of 16.97%. For the frigate, the generator heat input decreased from 1165.68 kW to 1003.64 kW, representing a reduction of 13.90%. This behavior results from increased internal heat recovery as the solution heat exchanger's effectiveness rises. The dilute solution leaving the absorber is preheated to a higher temperature before entering the generator, thereby reducing the required external heat input. The frigate

requires more generator heat than the corvette throughout the investigated range, while both vessels exhibit similar downward trends.

The solution heat exchanger transfers sensible heat from the hot concentrated solution leaving the generator to the colder dilute solution returning from the absorber. At fixed inlet conditions, increasing effectiveness allows a larger fraction of the available heat to be recovered. The dilute solution therefore enters the generator at a higher enthalpy, while the concentrated solution returns toward the absorber at a lower enthalpy. Since the generator outlet conditions remain fixed, preheating reduces the sensible heating required from the external heat source. This explains the decrease in generator heat input while maintaining the prescribed cooling capacity.

Figure 3 illustrates the effect of solution heat exchanger effectiveness on the refrigeration COP of the two vessels.

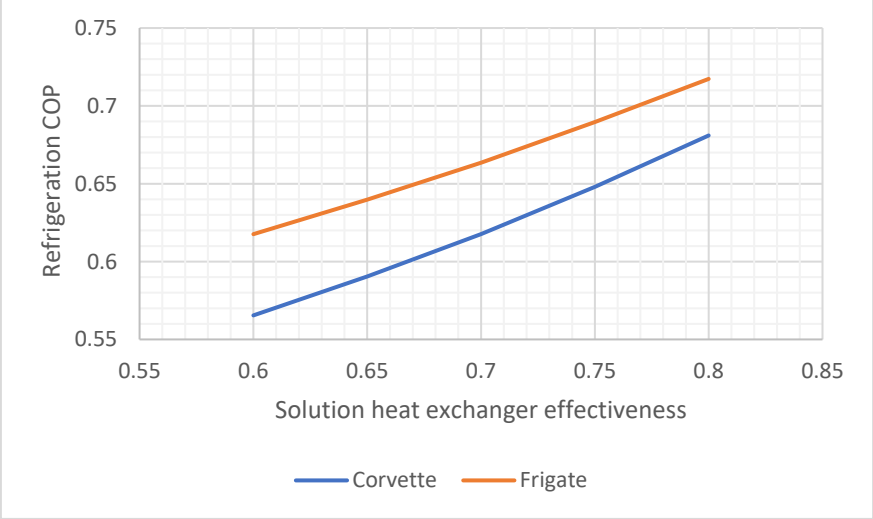


Figure 3. Effect of solution heat exchanger effectiveness on the refrigeration COP for the corvette and frigate.

As effectiveness increased from 0.60 to 0.80, the refrigeration COP rose from 0.565 to 0.681 for the corvette and from 0.617 to 0.720 for the frigate. These changes correspond to increases of approximately 20.5% and 16.7%, respectively. The main reason for the improvement in COP is the reduced generator heat requirement, resulting from increased internal heat recovery in the solution heat exchanger. As effectiveness increases, the dilute solution leaving the absorber enters the generator at a higher temperature, while the system's cooling capacity remains unchanged. As a result, less external heat input is required to achieve the same cooling effect. The frigate has a higher refrigeration COP than the corvette throughout the investigated effectiveness range, while both vessels show a similar upward trend.

The reduction in generator heat input and the increase in refrigeration COP agree with the trends reported by Ren et al. [42] for single-effect LiCl–H_2O and LiBr–H_2O systems. They found that increasing solution heat exchanger effectiveness improved internal heat recovery and reduced the external heat input. Their sensitivity analysis considered generator temperatures of 78–82 °C, compared with 90 °C in the present study. The agreement, therefore, concerns the direction of performance changes rather than identical COP values or percentage improvements.

Figure 4 illustrates the effect of solution heat exchanger effectiveness on the heat pump COP of the two vessels.

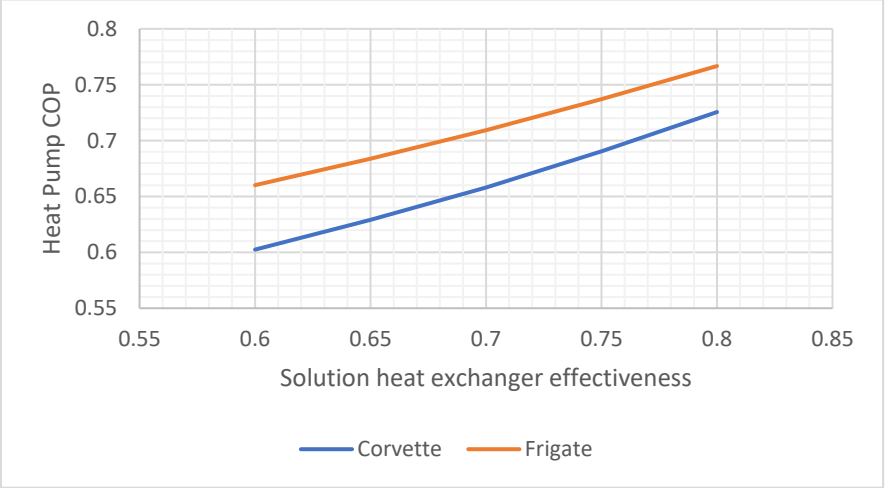


Figure 4. Effect of solution heat exchanger effectiveness on heat pump COP for the corvette and frigate.

As effectiveness increased from 0.60 to 0.80, the heat pump COP rose from 0.602 to 0.725 for the corvette and from 0.660 to 0.770 for the frigate. These changes correspond to increases of approximately 20.4% and 16.7%, respectively. The improvement in COP results from the reduced generator heat requirement due to greater internal heat recovery in the solution heat exchanger. As effectiveness increases, the dilute solution leaving the absorber enters the generator at a higher temperature. The heating capacity remains constant because the refrigerant mass flow rate and condenser inlet and outlet enthalpies do not change. This allows the same heating effect to be achieved with a lower external heat input. The frigate has a higher heat pump COP than the corvette throughout the investigated effectiveness range, while both vessels show a similar upward trend.

The COP increases in Figures 3 and 4 are governed by the relationship between internal heat recovery and external heat input. For each vessel, the prescribed cooling capacity and fixed refrigerant enthalpy difference across the evaporator determine a constant refrigerant mass flow rate. The fixed absorber and generator conditions also maintain the equilibrium solution concentrations and circulation ratio. Increasing effectiveness therefore raises the enthalpy of the solution entering the generator while preserving the refrigerant production required for cooling. The condenser heating capacity remains constant because the refrigerant flow rate and condenser inlet and outlet states are unchanged. The reduction in generator heat input thus increases the COP values for refrigeration and heat pumps.

Figure 5 illustrates the effect of solution heat exchanger effectiveness on the refrigeration exergy efficiency of the two vessels.

As effectiveness increased from 0.60 to 0.80, the refrigeration exergy efficiency rose from 0.239 to 0.288 for the corvette and from 0.199 to 0.231 for the frigate. These changes correspond to increases of approximately 20.5% and 16.1%, respectively. As the solution heat exchanger's effectiveness increases, internal heat recovery improves, and the generator's heat input decreases. Since the cooling capacity and evaporator operating conditions remain unchanged, the useful refrigeration exergy remains constant, while the exergy input associated with the heat supplied to the generator decreases. This reduction increases the system's refrigeration exergy efficiency. The corvette maintains a higher refrigeration exergy efficiency than the frigate throughout the investigated effectiveness range, while both vessels show a similar upward trend.

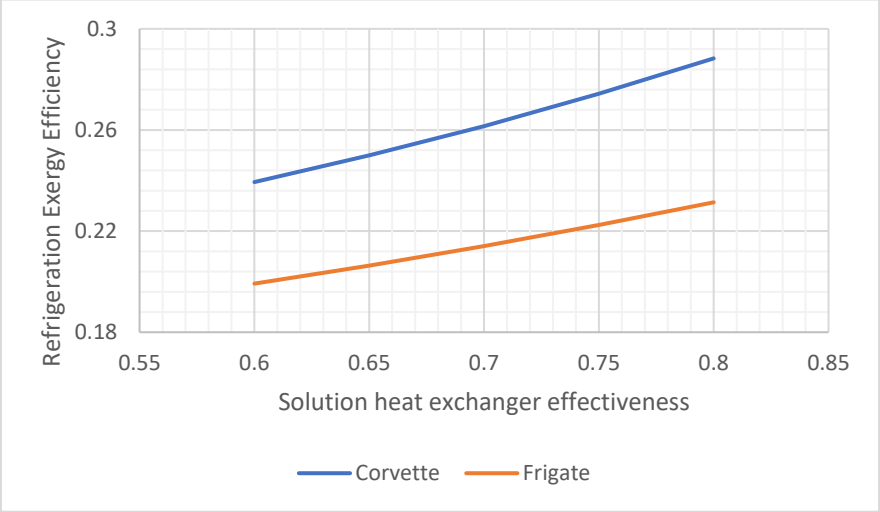


Figure 5. Effect of solution heat exchanger effectiveness on refrigeration exergy efficiency for the corvette and frigate.

Figure 6 illustrates the effect of solution heat exchanger effectiveness on the heat pump exergy efficiency of the two ships.

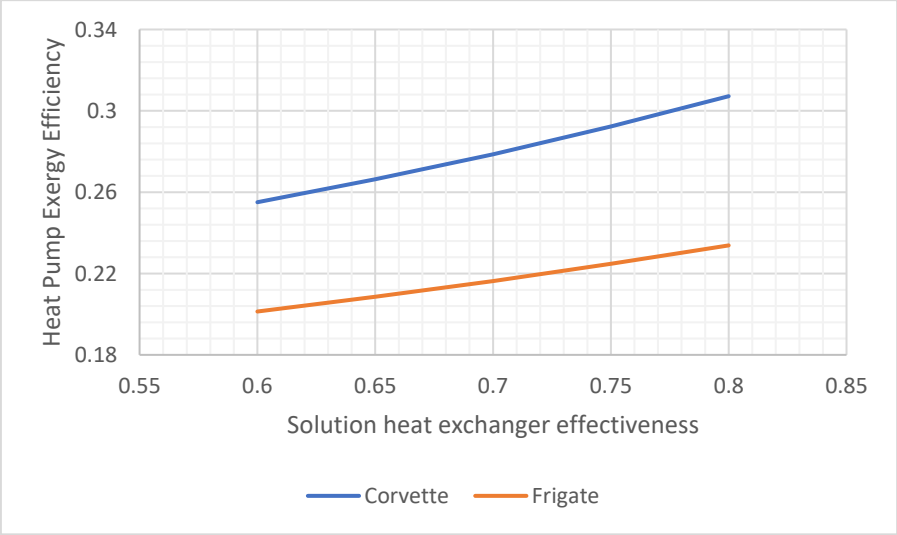


Figure 6. Effect of solution heat exchanger effectiveness on heat pump exergy efficiency for the corvette and frigate.

As the effectiveness value increased from 0.60 to 0.80, the heat pump exergy efficiency rose from 0.255 to 0.307 for the corvette and from 0.201 to 0.233 for the frigate. These changes correspond to increases of approximately 20.4% and 15.9%, respectively. Increasing the effectiveness of the solution heat exchanger improves heat recovery in the system, thereby reducing the generator's heat requirement. Since the system's heating capacity and operating temperatures remain constant, the useful heating exergy obtained at the condenser remains unchanged, while the exergy input associated with the heat supplied to the generator decreases; consequently, the heat pump exergy efficiency rises.

The increases in exergy efficiency shown in Figures 5 and 6 reflect the reduced external thermal input required to maintain the useful output. At fixed cooling and heating capacities and operating temperatures, the useful refrigeration and heating exergy remain constant. The temperature factor associated with the generator heat input also remains unchanged. Improved internal heat recovery reduces the generator heat

requirement and its associated exergy input, increasing the ratio of useful output exergy to supplied exergy. The improvement therefore results from meeting the same thermal demand with a smaller external exergy input.

The increase in refrigeration exergy efficiency is consistent with the findings of Rodríguez-Munoz et al. [47], who reported higher COP and exergy efficiency with greater solution heat exchanger effectiveness in both conventional and heat-recovery LiBr–H_2O absorption cycles. Improved internal heat recovery provides a common explanation for these trends. However, their working pair, cycle configurations, and operating conditions differ from those considered here, so the absolute efficiencies are not directly comparable.

The calculated saved fuel rate (kg/h), cost savings (USD/h), and reduced CO_2 emission (kg/h) remained unchanged over the investigated solution heat exchanger effectiveness range. Therefore, Figures 7–9 present a comparison between the two vessel classes.

Figure 7 compares the saved fuel flow rates for the corvette and frigate.

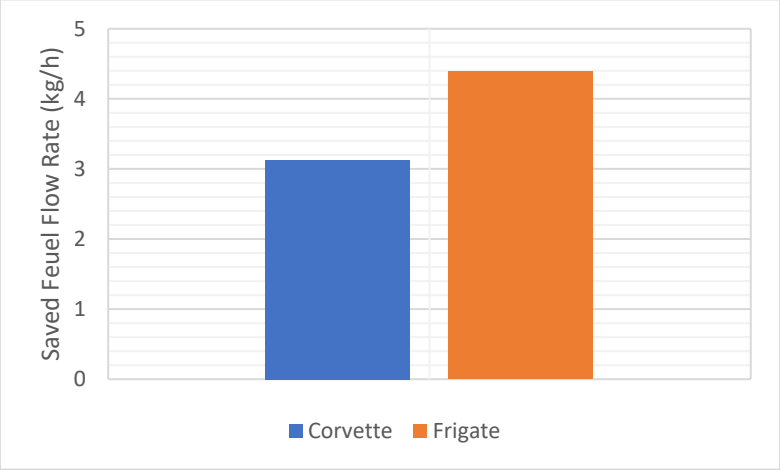


Figure 7. Comparison of the saved fuel flow rates for the corvette and frigate.

The saved fuel flow rate has been calculated to be 3.129 kg/h for the corvette and 4.393 kg/h for the frigate. The frigate therefore provides an additional fuel saving of 1.264 kg/h, representing a 40.4% higher fuel-saving rate than that of the corvette. This difference is mainly attributed to the frigate's greater heating and cooling demands, which require higher thermal energy input into the absorption system's generator. The recovery and utilization of gas turbine exhaust heat offset the energy that would otherwise have to be supplied through additional fuel consumption. Therefore, the larger amount of recovered heat utilized in the frigate application results in a higher equivalent fuel saving than in the corvette application.

Figure 8 compares the hourly fuel cost savings for the corvette and frigate.

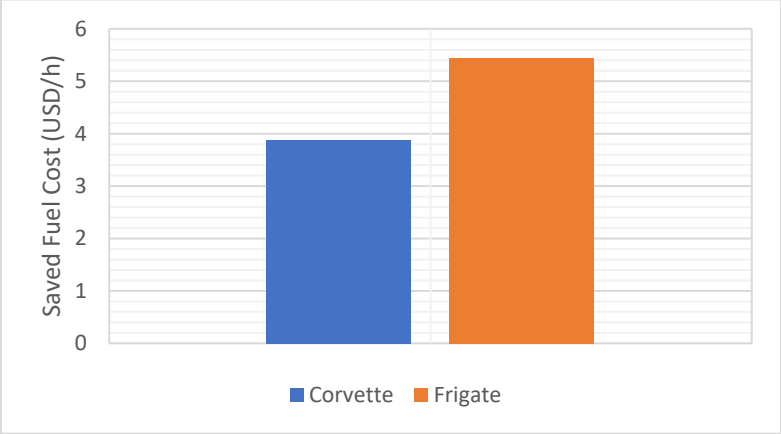


Figure 8. Comparison of fuel cost savings for the corvette and frigate.

Based on the assumed unit fuel price in the study, the fuel cost savings have been calculated to be 3.880 USD/h for the corvette and 5.447 USD/h for the frigate. The frigate application provides an additional cost saving of 1.567 USD/h compared with the corvette, corresponding to a 40.4% higher fuel cost savings. Since the fuel cost savings are directly proportional to the saved fuel flow rate, the higher fuel saving obtained for the frigate results in a proportional increase in economic benefit. This result indicates that utilizing gas turbine exhaust heat in the absorption system can provide greater economic benefits, particularly for vessels with higher heating and cooling demands.

Figure 9 compares the hourly CO_2 emission reductions for the corvette and frigate applications.

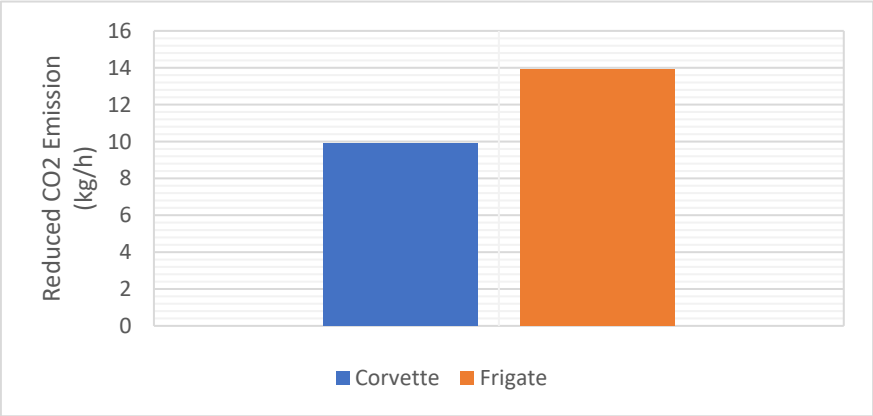


Figure 9. Comparison of reduced CO_2 emissions for the corvette and frigate.

The CO_2 emissions reductions have been calculated at 9.921 kg/h for the corvette and 13.926 kg/h for the frigate. The CO_2 emission reduction achieved for the frigate is 4.005 kg/h (40.4%) higher than that achieved for the corvette. Since the reduction in CO_2 emissions is calculated based on the amount of fuel saved and a constant emission factor, the percentage difference between the two vessels equals the difference in their fuel savings. The frigate's higher heating and cooling demands enable the absorption system to utilize more waste heat from the exhaust gas. This greater utilization of waste heat reduces the equivalent fuel requirement and yields a larger reduction in CO_2 emissions.

The estimated fuel savings and CO_2 emission reductions follow the same direction as those reported by Ozturk and Kandemir [40] for exhaust-driven LiBr–H_2O absorption systems on surface ships.

The results represent the fixed-temperature design conditions examined in this study. The effectiveness values shown in Figures 2–6 refer to the internal solution heat

exchanger rather than the seawater-cooled heat exchangers. In practice, seawater temperature affects heat rejection from the condenser and absorber. Previous LiCl–H_2O chiller simulations have shown that increasing cooling-water inlet temperature can reduce COP and cooling capacity [42]. Therefore, the improvements calculated here cannot be assumed to remain unchanged across different operating regions. Maintaining the assumed absorber temperature of 35 °C requires a sufficient temperature difference between the solution and the seawater. In heating mode, the assumed evaporator temperature of 4 °C similarly requires seawater conditions that allow heat transfer to the refrigerant.

For operation under changing seawater temperatures and thermal demands, possible control measures include adjusting secondary-circuit flow rates and regulating the heat supplied to the generator. The chilled-water supply temperature could serve as a control target in cooling mode. However, increasing seawater flow alone cannot maintain the assumed component temperatures when the available temperature difference is insufficient. Such conditions would require revised operating temperatures or additional cooling support. These control options have not been simulated in the present study. An off-design analysis incorporating seawater temperature, heat exchanger characteristics, and variable cooling demand is required to assess their performance.

Limitations and Applicability

The results represent steady-state design conditions at prescribed component temperatures and cooling loads. The improvements obtained by varying solution heat exchanger effectiveness therefore describe the influence of internal heat recovery under these conditions. Their magnitude may change with seawater temperature, available exhaust heat, and ship cooling demand. An application to a particular operating region requires checking whether the available heat source and seawater conditions can support the assumed generator, condenser, absorber, and evaporator temperatures.

The assumptions of equilibrium outlet states and negligible piping heat losses and pressure drops provide an idealized representation of the absorption cycle. Departures from equilibrium and additional thermal or hydraulic losses can alter the required heat input and auxiliary power, thereby affecting achievable performance. The calculated solution properties depend on the EES property functions, and their uncertainty has not been propagated into the reported results. The selected effectiveness range is a sensitivity interval rather than a verified operating envelope, particularly regarding solution crystallization. The fuel, cost, and emission results should also be interpreted as equivalent operating savings under the stated reference assumptions.

4. Verification

This section compares the calculated COP values for refrigeration and the heat pump with published results for LiBr–H_2O and LiCl–H_2O absorption systems. The comparison considers the working pairs, cycle configurations, operating conditions, and reported performance values, highlighting the similarities and differences between the studies.

The present system has been compared with the marine LiBr–H_2O absorption heat pump investigated by Ezgi [41], the single-effect LiCl–H_2O absorption refrigeration system examined by Ren et al. [42], and the LiCl–H_2O systems reported in [48,49]. The comparison uses the frigate case at a refrigeration capacity of 720 kW and a solution heat exchanger effectiveness of 0.80. The operating conditions and COP values are presented in Table 3.

Table 3. Comparison of the present system with the LiBr–H_2O and LiCl–H_2O absorption systems in the literature [41,42,48,49].

Parameter	This Study	[41]	[42]	[48]	[49]
Working pair	LiCl-H_2O	LiBr-H_2O	LiCl-H_2O	LiCl-H_2O	LiCl-H_2O
Q_{evap} (kW)	720	728.22	50	-	3.517
T_{gen} (°C)	90	90	80	115 (Heat source inlet)	78
T_{cond} (°C)	50	50	38	31 (Heat sink return)	36
T_{evap} (°C)	4	4	6	18 (Cooling fluid return)	10
T_{abs} (°C)	35	35	38	-	40
ε_{SHX}	0.80	0.80	0.70	-	0.7
COP_{ref}	0.72	0.70	0.73	0.61	0.7877
COP_{HP}	0.77	0.75	-	0.69	-

As shown in Table 3, the present system gives refrigeration and heat pump COP values of 0.720 and 0.770, compared with 0.70 and 0.75 reported by Ezgi [41]. The component temperatures and solution heat exchanger effectiveness are identical, and the refrigeration capacities are similar. However, the working pairs and exhaust heat sources differ. The higher COP values obtained in the present case, therefore, cannot be attributed solely to the replacement of LiBr with LiCl.

Ren et al. [42] reported a refrigeration COP of 0.730 using the same LiCl–H_2O working pair. Their lower condenser temperature and higher evaporator temperature provide a smaller refrigeration temperature lift, whereas the higher solution heat exchanger effectiveness in the present study improves internal heat recovery. The generator and absorber temperatures also differ between the studies. Ezgi's study therefore provides a comparison with a marine cooling–heating arrangement, while Ren's study provides a comparison using the same working pair.

The refrigeration and heat pump COP values reported in [48] are 0.61 and 0.69, respectively, both below the corresponding values obtained in the present study. However, the external fluid temperatures provided in [48] do not permit a direct comparison with the internal component temperatures of the present model. Reference [49] reports a refrigeration COP of 0.7877 at a refrigeration capacity of 3.517 kW. Its lower condenser temperature and higher evaporator temperature reduce the refrigeration temperature lift relative to the present system, although its generator temperature, absorber temperature, and solution heat exchanger effectiveness also differ. These comparisons place the calculated COP values within the range of the published results considered here, while the differences in operating conditions and temperature definitions limit their use as a direct quantitative validation.

5. Conclusions

This paper presents the findings of the thermodynamic assessment of the exhaust gas-driven LiCl–H_2O refrigeration and heat pump system for corvette and frigate applications. It highlights the influence of internal heat recovery, the estimated fuel and emission savings, and the limitations of the operating conditions examined.

Increasing the solution heat exchanger effectiveness from 0.60 to 0.80 improved internal heat recovery and reduced the generator heat requirement. The generator heat requirement decreased from 954.91 to 792.86 kW for the corvette and from 1165.68 to 1003.64 kW for the frigate. Over the same effectiveness range, the refrigeration COP increased from 0.565 to 0.681 for the corvette and from 0.617 to 0.720 for the frigate. The heat pump COP increased from 0.602 to 0.725 for the corvette and from 0.660 to 0.770 for the frigate. The exergy efficiencies followed the same trend. The refrigeration exergy efficiency increased from 0.239 to 0.288 for the corvette and from 0.199 to 0.231 for the frigate. The heat pump exergy efficiency increased from 0.255 to 0.307 for the corvette and from 0.201 to 0.233 for the frigate. Throughout the investigated effectiveness range, the

frigate had higher refrigeration and heat pump COP values, whereas the corvette had higher refrigeration and heat pump exergy efficiencies.

The saved fuel flow rate has been calculated to be 3.129 kg/h for the corvette and 4.393 kg/h for the frigate. These fuel savings corresponded to fuel cost savings of 3.880 USD/h for the corvette and 5.447 USD/h for the frigate. The hourly CO_2 emission reduction has been 9.921 kg/h for the corvette and 13.926 kg/h for the frigate. The saved fuel flow rate, fuel cost savings, and CO_2 emission reduction obtained for the frigate have been 40.4% higher than those obtained for the corvette.

The results show that the solution heat exchanger's effectiveness significantly influences the energy and exergy performance of the LiCl–H_2O absorption system. Recovering gas turbine exhaust heat reduces the equivalent fuel requirement and associated CO_2 emissions while enabling the same system to provide both cooling and heating. The proposed system, therefore, represents a promising option for improving energy efficiency and reducing the environmental impact of marine gas turbine-powered naval surface ships.

Future research should extend the model to variable seawater temperatures, gas turbine loads, and ship cooling and heating demands. An off-design model incorporating heat exchanger characteristics and pressure losses would help determine the conditions under which the prescribed thermal outputs can be maintained. The solution heat exchanger should be assessed in terms of achievable effectiveness, size, and the crystallization margin of the concentrated solution. Comparative calculations using LiCl–H_2O and alternative working pairs, including LiBr–H_2O, under identical operating conditions would help isolate the influence of working-pair selection. Experimental validation should include solution temperatures, concentrations, flow rates, component heat duties, and COP. Subsequent testing under representative ship operating conditions should examine mode switching and control strategies for maintaining the required supply-water temperature. Annual operating profiles and equipment costs should also be incorporated to assess fuel savings and the feasibility of investment.

Author Contributions: Investigation, H.K.; formal analysis, C.E.; methodology, H.K. and C.E.; project administration, H.K.; resources, H.K. and C.E.; validation, C.E.; writing—original draft, H.K.; writing—review and editing, C.E. All authors have read and agreed to the published version of the manuscript.

Funding: This research received no external funding.

Institutional Review Board Statement: Not applicable.

Informed Consent Statement: Not applicable.

Data Availability Statement: All data generated or analyzed during this study are included in this published article.

Conflicts of Interest: The authors declare no conflicts of interest.

Nomenclature

Roman symbols

$\dot{C}_{saved}$	Fuel cost saving rate (USD/h)
$COP_{absorption,REF}$	Absorption refrigeration coefficient of performance
$COP_{absorption,HP}$	Absorption heat pump coefficient of performance
$COP_{rev,REF}$	Reversible absorption refrigeration coefficient of performance
$COP_{rev,HP}$	Reversible absorption heat pump coefficient of performance
CR	Solution circulation ratio
h_{in}	Inlet specific enthalpy (kJ/kg)

h_{out}	Outlet specific enthalpy (kJ/kg)
H_u	Fuel lower heating value (kJ/kg)
$\dot{m}_{in}$	Inlet mass flow rate (kg/s)
$\dot{m}_{out}$	Outlet mass flow rate (kg/s)
$\dot{m}_r$	Refrigerant mass flow rate (kg/s)
$\dot{m}_{ss}$	Strong solution mass flow rate (kg/s)
$\dot{m}_{ws}$	Weak solution mass flow rate (kg/s)
T_H	Heated-space temperature (K)
T_L	Refrigerated-space temperature (K)
T_0	Environmental reference temperature (K)
T_s	Heat-source temperature (K)
$\dot{W}_{comp}$	Reference-system compressor power input (kW)
$\dot{W}_{net}$	Net power saving (kW)
$\dot{W}_{pump}$	Solution pump power input (kW)
x_{in}	Inlet salt mass fraction
x_{out}	Outlet salt mass fraction
x_{ss}	Salt mass fraction of the strong solution
x_{ws}	Salt mass fraction of the weak solution
Greek symbols	
η_{DG}	Diesel generator electrical efficiency
Abbreviations or formulas	
CII	Carbon Intensity Indicator
CO_2	Carbon dioxide
COP	Coefficient of performance
EES	Engineering Equation Solver
EEXI	Energy Efficiency Existing Ship Index
H_2O	Water
LiBr	Lithium bromide
LiCl	Lithium chloride
ORC	Organic Rankine Cycle
USD	United States dollar
US NSD	United States Navy Standard Day

References

1. Wang, T.; Cheng, P.; Zhen, L. Green development of the maritime industry: Overview, perspectives, and future research opportunities. *Transp. Res. Part E Logist. Transp. Rev.* **2023**, *179*, 103322.
2. Tadros, M.; Ventura, M.; Guedes Soares, C. Review of current regulations, available technologies, and future trends in the green shipping industry. *Ocean Eng.* **2023**, *280*, 114670.
3. Zanobetti, F.; Pio, G.; Jafarzadeh, S.; Munoz Ortiz, M.; Cozzani, V. Decarbonization of maritime transport: Sustainability assessment of alternative power systems. *J. Clean. Prod.* **2023**, *417*, 137989.
4. Liu, P.; Xu, Y.; Xie, X.; Turkmen, S.; Fan, S.; Ghassemi, H.; He, G. Achieving the global net-zero maritime shipping goal: The urgencies, challenges, regulatory measures and strategic solutions. *Ocean Coast. Manag.* **2024**, *256*, 107301.
5. Ap Dafydd Tomos, B.; Stamford, L.; Welfle, A.; Larkin, A. Decarbonising international shipping—A life cycle perspective on alternative fuel options. *Energy Convers. Manag.* **2024**, *299*, 117848.
6. Hu, K.; Liu, X.; Chen, Y.; He, D. Influence of marine conditions on thermal efficiency of SCO_2 Brayton cycle for waste heat recovery. *Appl. Therm. Eng.* **2023**, *227*, 120391.
7. Zhang, Q.; Wang, S.; Pan, D.; Li, J. Investigation on thermo-economic performance of shipboard waste heat recovery system integrated with cascade latent thermal energy storage. *J. Energy Storage* **2023**, *64*, 107171.
8. Dadpour, D.; Gholizadeh, M.; Estiri, M.; Poncet, S. Multi objective optimization and 3E analyses of a novel supercritical/transcritical CO_2 waste heat recovery from a ship exhaust. *Energy* **2023**, *278*, 127843.
9. Hellström, M.; Rabetino, R.; Schwartz, H.; Tsvetkova, A.; Haq, S.H.U. GHG emission reduction measures and alternative fuels in different shipping segments and time horizons—A Delphi study. *Mar. Policy* **2024**, *160*, 105997.

10. Liu, Z.; Lu, D.; Shen, T.; Guo, H.; Bai, Y.; Wang, L.; Gong, M. New configurations of absorption heat transformer and refrigeration combined system for low-temperature cooling driven by low-grade heat. *Appl. Therm. Eng.* **2023**, *228*, 120567.
11. Gao, H.; Huang, J.; Zhai, J.; Hu, Y.; Yan, Y. Advance and technical prospects of membrane-based absorption refrigeration system: A comprehensive review. *J. Ind. Eng. Chem.* **2026**, *156*, 210–231.
12. Pacheco-Cedeno, J.S.; Rodríguez-Munoz, J.L.; Ramírez-Minguela, J.J.; Perez-García, V. Comparison of an absorption-compression hybrid refrigeration system and the conventional absorption refrigeration system: Exergy analysis. *Int. J. Refrig.* **2023**, *155*, 81–92.
13. Lu, D.; Jiang, W.; Liu, Z.; Guan, X.; Zhang, Z.; Bai, Y.; Zhang, X.; Qin, J.; Gong, M. Study on the ammonia-water two-stage evaporation absorption refrigeration system for the cooling process with temperature-distributed heat load. *Int. J. Refrig.* **2023**, *151*, 125–135.
14. Liang, A.; Yang, S.; Ding, Y.; Ma, S. Triple effect absorption refrigeration systems for the deep recovery of low grade waste heat. *Appl. Therm. Eng.* **2024**, *250*, 123500.
15. Ji, L.; Shukla, S.K.; Zuo, Z.; Lu, X.; Ji, X.; Wang, C. An overview of the progress of new working pairs in absorption heat pumps. *Energy Rep.* **2023**, *9*, 703–729.
16. Kallitsis, K.; Koulocheris, V.; Pappa, G.; Voutsas, E. Evaluation of water+imidazolium ionic liquids as working pairs in absorption refrigeration cycles. *Appl. Therm. Eng.* **2023**, *233*, 121201.
17. Zhang, X.; Cai, L.; Chen, T.; Liu, J.; Zhang, X. Thermodynamic screening and analysis of ionic liquids as absorbents paired with low-GWP refrigerants in absorption refrigeration systems. *Energy* **2023**, *282*, 128414.
18. Gao, Z.; Zhu, H.; Zhang, X.; Wang, L.; Zhang, C. Experimental study on a novel pumpless absorption refrigeration system using R134a/DMF as working pair. *Int. J. Refrig.* **2024**, *166*, 119–128.
19. Cheng, X.; Yin, Y. Performance analysis and optimization of a coupled open and close liquid desiccant sorption system using LiCl solution. *Appl. Therm. Eng.* **2023**, *233*, 121153.
20. Zhai, C.; Wu, W. Experimental parameter study and correlation development of microchannel membrane-based absorption process for efficient thermal cooling with high compactness. *Energy* **2023**, *279*, 128080.
21. Rodríguez-Munoz, J.L.; Ramírez-Minguela, J.J.; Ituna-Yudonago, J.F.; Gonzalez-Hernandez, I.J. Performance improvement by rectifier heat integration in an alternative absorption-compression hybrid refrigeration system. *Appl. Therm. Eng.* **2025**, *277*, 127139.
22. Wang, Y.; Kong, H.; Zhu, H.; Gao, P.; Wu, W.; Wang, L. Compression-assisted absorption refrigeration cycle employing organic working pairs for ultra-low grade heat recovery. *Int. J. Refrig.* **2024**, *165*, 485–499.
23. Du, S.; Xu, Z.; Wang, R.; Yang, C. Development of direct seawater-cooled LiBr–H_2O absorption chiller and its application in industrial waste heat utilization. *Energy* **2024**, *294*, 130816.
24. Huang, C.; Shao, S.; Wang, N.; Guo, Y.; Wu, W. Performance analysis of compression-assisted absorption refrigeration-heating system for waste heat recovery of liquid-cooling data center. *Energy* **2024**, *305*, 132325.
25. Fisher, R.; Ciappi, L.; Niknam, P.; Braimakis, K.; Karellas, S.; Frazzica, A.; Sciacovelli, A. Innovative waste heat valorisation technologies for zero-carbon ships—A review. *Appl. Therm. Eng.* **2024**, *253*, 123740.
26. Barone, G.; Buonomano, A.; Del Papa, G.; Maka, R.; Palombo, A. Enhancing shipboard waste heat management with advanced technologies. *Renew. Sustain. Energy Rev.* **2025**, *208*, 114871.
27. Diaz-Secades, L.A.; Gonzalez, R.; Rivera, N.; Montanes, E.; Quevedo, J.R. Waste heat recovery system for marine engines optimized through a preference learning rank function embedded into a Bayesian optimizer. *Ocean Eng.* **2023**, *281*, 114747.
28. Diaz-Secades, L.A.; Gonzalez, R.; Rivera, N.; Quevedo, J.R.; Montanes, E. Parametric study of organic Rankine working fluids via Bayesian optimization of a preference learning ranking for a waste heat recovery system applied to a case study marine engine. *Ocean Eng.* **2024**, *306*, 118124.
29. Gubba, S.R.; Kodaboina, R.V.; Kenkoh, K.Y.; Fernandes, R.; Turner, J.W.G. A Joule cycle-based approach to recover waste heat from marine and heavy-duty vehicles. *Energy* **2025**, *337*, 138755.
30. Qin, L.; Xie, G.; Ma, Y.; Li, S. Thermodynamic analysis and multi-objective optimization of a waste heat recovery system with a combined supercritical/transcritical CO_2 cycle. *Energy* **2023**, *265*, 126332.
31. Alkotami, A.; Elattar, H.F.; Fouda, A. Performance analysis of a novel marine engine waste heat recovery system for combined power and cooling generation. *Appl. Therm. Eng.* **2025**, *281*, 128604.
32. Ouyang, T.; Pan, M.; Tan, X.; Huang, Y.; Mo, C.; Wang, Z. Advanced power-refrigeration-cycle integrated WHR system for marine natural gas engine base on multi-objective optimization. *Energy* **2023**, *283*, 129038.

33. Que, W.; Li, X.; Chen, X.; Pan, M.; Fu, C.; Liang, L.; Su, T. Potential of solid oxide fuel cells as marine engine assisted by combined cooling and power cogeneration systems. *Appl. Therm. Eng.* **2024**, *254*, 123821.
34. Chun, A.; Donatelli, J.L.M.; Santos, J.J.C.S.; Zabeu, C.B.; Carvalho, M. Superstructure optimization of absorption chillers integrated with a large internal combustion engine for waste heat recovery and repowering applications: Thermodynamic and economic assessments. *Energy* **2023**, *263*, 125970.
35. Mubashir, W.; Adnan, M.; Zaman, M.; Imran, M.; Naqvi, S.R.; Mehmood, A. Thermo-economic evaluation of supercritical CO_2 Brayton cycle integrated with absorption refrigeration system and organic Rankine cycle for waste heat recovery. *Therm. Sci. Eng. Prog.* **2023**, *44*, 102073.
36. Salilih, E.M.; Bamaga, O.; Almatrafi, E.; Abulkhair, H.; Alhumade, H.; Bamasag, A.; Ahmed, I.; Alsaiari, A.; Nurrohman; Albeirutty, M. Performance analysis of a novel absorption-refrigeration driven membrane condenser system for recovery of water and waste heat from flue gas. *Int. J. Refrig.* **2023**, *156*, 219–231.
37. Zhang, J.; Mei, N.; Yuan, H. Design, analysis, and operation optimisation of a shipborne absorption refrigeration–ice thermal storage system based on waste-heat utilization. *Therm. Sci. Eng. Prog.* **2024**, *53*, 102720.
38. Radchenko, R.; Radchenko, A.; Mikielewicz, D.; Radchenko, M.; Pavlenko, A.; Andreev, A. Adaptable management for cooling cyclic air in ship power plants by heat conversion—Part 1: Downsizing strategy for cogeneration plants. *Energy* **2024**, *313*, 133845.
39. Mugabi, J.; Yu, J.; Jeong, J.-H. Thermodynamic feasibility and system-level performance assessment of integrated scavenge-air cooling and waste-heat-driven absorption refrigeration for marine engines. *Energy* **2026**, *360*, 141413.
40. Ozturk, O.; Kandemir, I. Analysis of single and double effect LiBr-H_2O absorption cooling systems to meet the cooling requirements of surface ships. *Appl. Therm. Eng.* **2025**, *262*, 125206.
41. Ezgi, C. Design and thermodynamic analysis of an H_2O–LiBr AHP system for naval surface ship application. *Int. J. Refrig.* **2014**, *48*, 153–165.
42. Ren, J.; Qian, Z.; Yao, Z.; Gan, N.; Zhang, Y. Thermodynamic evaluation of LiCl-H_2O and LiBr-H_2O absorption refrigeration systems based on a novel model and algorithm. *Energies* **2019**, *12*, 3037.
43. Lei, T.; Qian, Z.; Ren, J. Performance evaluation of LiBr-H_2O and LiCl-H_2O working pairs in compression-assisted double-effect absorption refrigeration systems for utilization of low-temperature heat sources. *Energies* **2023**, *16*, 6036.
44. Klein, S.; Alvarado, F. *Engineering Equation Solver (EES)*; F-Chart Software, LLC: Madison, WI, USA. Available online: https://www.fchart.com/ees/ (accessed on 12 June 2026).
45. Fiscal Year 2026 Standard Fuel Price Change. Available online: https://www.dla.mil/energy/business/standard-prices/ (accessed on 19 August 2026).
46. Ezgi, C. Design and Analysis of a NATO F-76 Diesel-Fueled Solid Oxide Fuel Cell System on Naval Surface Ship. Ph.D. Thesis, Ege University, Izmir, Turkey, 2009.
47. Rodríguez-Muñoz, J.L.; Pacheco-Cedeño, J.S.; Ituna-Yudonago, J.F.; Ramírez-Minguela, J.J.; González-Hernández, I.J. First and Second Law Analysis of a LiBr-Water Absorption Cycle with Recovering Condensation Heat for Generation. *Front. Heat Mass Transf.* **2024**, *22*, 1719–1741.
48. Oberweis, S.; Al-Shemmeri, T. Performance Evaluation of a Lithium-Chloride Absorption Refrigeration and an Assessment of Its Suitability for Biomass Waste Heat. *Appl. Sci.* **2012**, *2*, 709–725.
49. Patel, J.; Pandya, B.; Mudgal, A. Exergy Based Analysis of LiCl-H_2O Absorption Cooling System. *Energy Procedia* **2017**, *109*, 261–269.

Disclaimer/Publisher's Note: The statements, opinions and data contained in all publications are solely those of the individual author(s) and contributor(s) and not of MDPI and/or the editor(s). MDPI and/or the editor(s) disclaim responsibility for any injury to people or property resulting from any ideas, methods, instructions or products referred to in the content.